Macromolecules

ARTICLE

pubs.acs.org/Macromolecules

Helix Formation in the Polymer Brush

Mark Kastantin*,† and Matthew Tirrell‡

†Department of Chemical & Biological Engineering, University of Colorado, Boulder, Colorado 80309, United States

‡Department of Bioengineering, University of California, Berkeley, California 94720, United States

ABSTRACT: This work considers the physics of a brush formed by polymers capable of undergoing a helix−coil transition. A self-consistent field approximation for strongly stretched polymer chains is used in combination with a lattice model of the interaction energy in helix−coil mixtures. Crowding-induced chain stretching stabilizes helix formation at moderate tethering densities while high tethering density causes sufficiently strong stretching to unravel segments of the helix, resulting in distinct layers of monomer density and helical content. Compared to a random-coil brush at low-to-moderate tethering density, a helicogenic brush is less resistant to compression in the direction perpendicular to stretching due to easy alignment of helices and fewer unfavorable interactions between helical segments. At higher tethering density, the above-mentioned stretch-induced decrease in helical content resists further compression. The proposed model is useful for understanding an emerging class of biomaterials that utilize helix-forming polymer brushes to induce shape changes or to stabilize biofunctional helical peptide sequences.

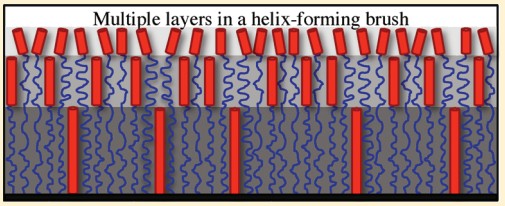

INTRODUCTION

Biomaterials are becoming increasingly sophisticated through the exploitation of polymers that are capable of undergoing transitions in secondary structure.[1−3] In one class of biomaterials, helicogenic polymers may be used in stimuli-responsive shape changing materials. For example, polylysine-polybutadiene block copolymers have been shown to form micelles in aqueous solution that undergo transitions from spheres to rods upon increasing pH, and this shape transition correlates with a helix−coil transition in the polylysine block.[4] Related block copolymers with a smaller polylysine block were shown to form vesicles in which the morphology was dependent on secondary structure in polylysine.[5] Similar phenomena were observed in ethanol using poly(γ-benzyl L-glutamate)−poly(ethylene glycol) graft copolymers in which addition of trifluoroacetic acid caused α-helices to return to the random-coil state. This led to a transition from spindle-like micelles to larger aggregates.[6] On a solid surface, end-tethered polylysine brushes were shown to interconvert between random coils, α-helices, and even β-sheets in response to complexation with anionic polymers in aqueous solution.[7] In the above examples, the effects of helix formation on micelle geometry can be qualitatively rationalized as helices decreasing brush resistance to increasing tethering density. As a result, the effective area of the headgroup decreases, thereby increasing the shape-determining packing parameter and driving a transition to flatter structures.[8]

In a second class of biomaterials, brush formation is used to stabilize helical structure and increase biofunctionality. In the work of Tu et al., a 37-residue peptide was predominantly a random-coil in solution but regained helical structure upon tethering to an alkyl tail that directed self-assembly into rod-like micelles.[9] Perhaps more importantly, helical structure was linked to the ability of the peptide to bind DNA, making brush effects critical to the biofunctionality of the micelle. This helical stabilization can be explained by the crowding-induced stretching of chains in a brush decreasing the conformational freedom of a random-coil monomer and lowering the entropic barrier to helix formation. Also within this class, other types of secondary structures have been stabilized by brush formation (e.g., β-sheets and triple-helices); the present work focuses solely on single-helix formation.[10,11]

While qualitative explanations exist for secondary structure-induced shape changes and brush-induced helix stabilization, quantitative models of these effects are sparse. Buhot and Halperin presented a model for a helicogenic brush and demonstrated that the brush state should both sharpen the helix−coil transition and shift it to higher temperature (i.e., stabilize the helical state).[12] Their model assumed that an individual chain existed either in a completely helical or completely random-coil state. Helices were modeled as rigid rods that were perfectly oriented normal to the grafting surface and immersed completely by the surrounding coils. This last assumption limited the model to short chains where the radius of gyration of the random-coil is larger than the length of the helix. Consequently the upper limit on chain length, N, is given by $N_{max} \leq 2(a/a_h)^2$ where a is the coil monomer length, a_h is the projection of the monomer length along the axis of the helix, and the factor of 2 accounts for the fact the grafting process stretches a random-coil in the direction normal to the surface even at low surface coverage. For a = 3.8 Å and a_h = 1.5 Å, N_{max} = 13, which is a restrictive assumption for the systems motivating the present work.

Received: April 4, 2011
Revised: May 13, 2011
Published: June 02, 2011

In contrast, this work considers a brush consisting of long chains capable of forming α-helices anywhere along the length of a given chain. Individual chains are allowed to stretch nonuniformly as a function of distance from the grafting surface, yielding a continuous distribution of chain ends throughout the brush. Given that stretching has been demonstrated to affect the helix−coil transition,[12,13] nonuniform stretching implies that a polypeptide can be induced to form helices nonuniformly along its length. Put another way, stretching and helix formation balance each other locally, rather than along the entire length of the chain.

This view of the brush is handled using a self-consistent field approximation for highly stretched chains as developed by Milner, Witten, and Cates and later expanded by Shim and Cates.[14,15] In this method, the elastic energy to stretch a segment of the chain must be specified as well as the interaction energy between polymer segments as a function of density. It has predicted force−distance profiles in excellent quantitative agreement with experimental data in addition to being confirmed by Monte Carlo and molecular dynamics simulations.[16−20] More importantly, self-consistent field methods have the capability to resolve brush microstructure such as nonuniform monomer density profiles and, in the present work, local variations in helical content. For the elastic energy, helices are modeled as wormlike chains and random-coil segments of the polypeptide are described using the freely jointed chain model, thus giving the entire polypeptide finite extensibility as a function of the number of helical residues.[13] Repulsive monomer−monomer interactions are incorporated via a lattice model of an athermal tertiary mixture of rods, coils, and solvent.[21−23] The goal of the present work is to move toward a realistic, generally applicable model of helicogenic brushes in order to explain experimental observations while providing a framework to predict and control the responsiveness of these systems. While substantial numerical manipulation is required for the polypeptide chains considered here, the method is sufficiently general so that other systems of interest may be treated similarly.

THEORY

Consider a flat polymer brush consisting of monodisperse chains of N monomers. Chains are end-grafted at a grafting density of Σ chains per unit area and have a position-dependent monomer concentration in solution of ρ monomers per unit volume. Each monomer has a characteristic length, a. Chains are stretched away from the surface along the Z-axis by a stretching force, b, which is caused by crowding from nearby chains rather than an externally applied force. For this work, it is convenient to use nondimensional variables to describe the brush. The Z-coordinate will be normalized by the contour length of the chain (Na) and the new nondimensional coordinate will therefore be $z = Z/Na$. All other parameters of the brush in this direction (e.g., chain starting height and total brush height) will also be in units of Na. The nondimensional stretching force will be defined as $x = ba/kT$ where k is Boltzmann's constant and T is absolute temperature. Similarly, all energies (e.g., elastic, interaction, overall brush energy) will be in units of kT per-monomer. The nondimensional tethering density will be $\sigma = a^2\Sigma$ and the nondimensional volume fraction will be $\phi = \rho/a^3$. The position along the chain will be given nondimensionally as $n = t/N$ where t is the position along the chain in monomer units. Finally, any section of chain may consist of monomers in both helical and random-coil states. The monomer fraction in the helical state will be called θ.

This work will develop a model of a helicogenic polymer brush that balances osmotic repulsion and elastic chain stretching locally. This local balance was done self-consistently by Milner, Witten, and Cates (MWC) in a manner that was analytically tractable in the original version of their theory.[14] However, the form for osmotic repulsion required to achieve analytical results limits the validity of the model to moderate density and weak excluded volume. A more general extension of the MWC method was developed shortly thereafter by Shim and Cates (SC) in order to handle finite extensibility and density saturation effects.[15] This second approach will be used here because it can handle arbitrary forms of the elastic free energy and monomer−monomer interactions, a feature that is useful when describing a helicogenic brush. In contrast, the MWC method uses a binary form of monomer−monomer interaction energy and Gaussian elasticity, while a similar theory developed by Zhulina et al.[24,25] allows for arbitrary interaction energy but still uses Gaussian elasticity. This section will first outline the SC method then proceed to develop appropriate forms of the elastic stretching energy and osmotic repulsion to describe the brush. Finally, the section will conclude with a discussion on the integration of these components to determine the space-dependent monomer density, helical content, and orientation profiles.

A Self-Consistent Field Approach to the Polymer Brush. This section briefly outlines the practical aspects of the SC method; refs 14 and 15 should be consulted for further detail. The basic assumption of the MWC and SC methods is that polymer chains in a brush are strongly stretched, such that fluctuations around the most probable trajectory may be neglected. In order to determine the most probable trajectory, the overall free energy of the brush is minimized by minimizing the "action" on each chain. This requirement is satisfied by the Euler−Lagrange equations for each chain where the Lagrangian is given by $F_{el}(\dot{z},z,n) - V(z)$. Here, $\dot{z}$ is the local stretching of the chain given by dz/dn, z is the distance from the grafting surface, n is the position along the chain and $V(z)$ is the negative of the space-dependent monomer chemical potential as will be discussed later. Thus, each chain must satisfy:

$$-\frac{\partial V(z)}{\partial z} = \frac{\partial}{\partial n}\left(\frac{\partial F_{el}}{\partial \dot{z}}\right)$$

If $\partial F_{el}/\partial \dot{z}$ does not depend explicitly on n, there exists a constant, H, such that

$$H = \dot{z}\frac{\partial F_{el}}{\partial \dot{z}} - F_{el} + V(z)$$

H may also be equated to the total energy, $V(\zeta)$ where ζ is the starting height of the chain, to give an expression for $\Delta V = V(\zeta) - V(z)$. For future convenience, U will be defined as $U(z) = V(z) - V(h) + A(h)$ where A is a function of the brush height, h and thus:

$$\Delta U = \Delta V = \dot{z}\frac{\partial F_{el}}{\partial \dot{z}} - F_{el} \qquad (1)$$

Equation 1 defines $\dot{z}$ as a function of ΔU and can be used to satisfy the "equal time" constraint requiring that all chains use the same number of monomers to traverse the chain trajectory from the distal chain end (at a height of $z = \zeta$) to the grafting surface. This "equal time" constraint is given in eq 2 where the integration is

performed in U-space and $f(U') = dz/dU'$ is the unknown function to be determined. Determination of dz/dU and subsequent integration with the boundary condition $U(0) = 0$ yields $U(z)$.

$$\int_0^U dU' f(U')\dot{z}^{-1}(U - U') \tag{2}$$

In general, eq 2 may be solved through the use of Laplace transform methods. This process is complicated in the present work because $\dot{z}$ is nonanalytical and exhibits a discontinuity in its first derivative due to the helix−coil transition. Numerical inversion of the Laplace transform is possible by any of several powerful numerical algorithms[26,27] whose utility for polymer statistical mechanics has recently been demonstrated.[28] However, the discontinuous first derivative in $\dot{z}$ implies singularities in f. In order to handle this, the resolution of the numerical routine is increased in the vicinity of the singularities such that eq 2 is satisfied to within 2%. Greater numerical resolution significantly increases computational effort while only slightly increasing accuracy.

The balance between stretching and osmotic repulsion is performed at this point by specifying $V(z)$ via a density-dependent equation of state, $F_{int}(\phi)$, as shown in eq 3 with ϕ being the monomer volume fraction:

$$V(z) = -\frac{\delta F_{\text{int}}(\phi)}{\delta \phi} \tag{3}$$

Thus, the density profile can be determined for a given value of $A(h)$ as shown in eq 4:

$$U(z) = -\frac{\delta F_{\text{int}}(\phi)}{\delta \phi} + \left.\frac{\delta F_{\text{int}}(\phi)}{\delta \phi}\right|_h + A(h) \tag{4}$$

Conservation of material is used to fix $A(h)$ as shown in eq 5 where σ is the total nondimensional surface density of grafted chain:

$$\sigma = \int_0^h dz\, \phi(z) \tag{5}$$

Thus, $A(h)$ may be determined as a function of σ, allowing the overall brush free energy to be calculated as shown in eq 6:

$$F_{br} = \frac{1}{\sigma}\int_0^\sigma d\sigma'\, A(\sigma') \tag{6}$$

Finally, the probability distribution of chain ends, $\varepsilon(z,h)$ is given by eq 7:

$$\varepsilon(z,h) = \frac{1}{\sigma}\frac{dU(z)}{dz}\int_{U(z)}^{U(h)} dU' \frac{d\phi}{dU'} f(U' - U(z)) \tag{7}$$

Local Balance between Stretching and Helix Formation. Because of the variation in stretching along the length of a chain, it is assumed that helix formation and stretching equilibrate locally. To quantify these effects, this work adopts a modified form of the analysis developed by Buhot and Halperin.[13] Coil segments of the chain are modeled as freely jointed chains while helices are modeled using a variational approximation to the wormlike chain model. In this treatment, there is no dependence of the elastic free energy on the number or size of helical domains. With this in mind, the elastic free energy of a segment of chain under an applied force is given in the fixed distance ensemble by eq 8 where θ is the fraction of helical monomers, x is the reduced force as previously defined, α is a force-dependent variational parameter, $\gamma = a/a_h = 0.4$, and $\eta = 1000$ is the persistence length of the wormlike chain in units of monomers:

$$F_{el} = \dot{z}x - (1-\theta)L_{\text{int}}(x) - \frac{\theta}{4\eta}(4\eta x\gamma - \alpha)L(\alpha) \tag{8}$$

The Langevin function, L, and its integral, L_{int} are given as $L(x) = \coth x - 1/x$ and $L_{int} = \ln[(\sinh x)/x]$, respectively. The reduced force and its associated variational parameter, α, can be expressed in terms of $\dot{z}$ using eqs 9 and 10:

$$\dot{z} = (1-\theta)L(x) + \theta\gamma L(\alpha) \tag{9}$$

$$4\eta x\gamma - \alpha = L(\alpha)/(\alpha^{-2} - \sinh^{-2}(\alpha)) \tag{10}$$

Regarding the free energy of helix formation, Buhot and Halperin adapt the Zimm−Bragg formalism to account for polydispersity among helical domains. In the context of local helix formation, however, the current work assumes that while a short section of chain may be partially helical, there is only one helical and one coil domain in that section and the entropy of helix placement is negligible. Furthermore, the free energy associated with the helix−coil interface is set to zero, causing the Zimm−Bragg cooperativity parameter to go to 1 (i.e., no cooperativity of the helix−coil transition). This was done for two reasons. The first is that a cooperative transition implies the specification of a chain length (and subsequent correlation volume in the brush) in which stretching and osmotic repulsion will balance. While intrachain correlations may be incorporated into future generations of this model, there is currently no simple framework for doing so. Second, it is unclear that a helix−coil transition within a single chain is as cooperative in the brush as it is in solution. The penalty associated with a helix−coil interface is often attributed to the loss of conformational entropy of the monomer without as much of the free energy benefit gained by helix formation either due to hydrogen bonding interactions, or more likely, due to the liberation of water necessary to solvate the coil monomer. In a dense brush, loss of monomer entropy upon helix formation is likely to be less significant and it is also possible that the benefit of water liberation may not be as important as in bulk solution. With this in mind, the free energy of helix formation (F_{hf}) is given simply in eq 11:

$$F_{hf} = -\theta \ln(s) \tag{11}$$

Here the Zimm−Bragg parameter is $s = \exp(-\Delta g/kT)$ and Δg is the free energy change experienced by a monomer moving from the coil to helical state such that $s > 1$ indicates that the helical state is favored.

Helix formation and stretching equilibrate locally by the minimization condition given by eq 12 where θ^* denotes the fraction of helical monomers at local equilibrium. Subsequently, equilibrium θ^* is implied and the superscript is not used.

$$\left.\frac{d(F_{hf} + F_{el})}{d\theta}\right|_{\theta^*} = 0 \tag{12}$$

It should be noted that no special treatment is given to helical sections placed at the grafting surface ($z = 0$). While acknowledging that the surface can influence helix formation in the near-surface monomers,[12] long chains are the primary focus of this work. Consequently, while this model may not capture the brush microstructure at very small z, this region is expected to have a negligible effect on microscopic brush properties away from the

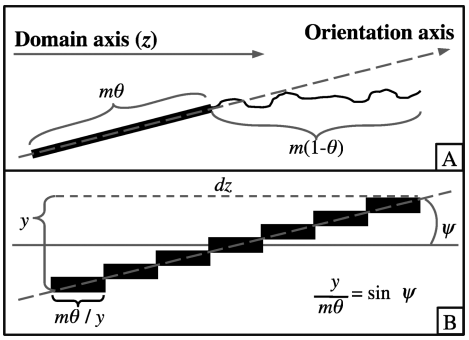

Figure 1. (A) Section of a polymer chain with m monomers consisting of one helical segment (dark rectangle) with $m\theta$ monomers and one random-coil (thin line) segment with $m(1-\theta)$ monomers. (B) Helical segment oriented with angle, ψ, to the domain axis. This helix can be approximated as a series of smaller helices of length $m\theta/y$ that are each perfectly oriented with the domain axis.

surface and on macroscopic properties such as compressibility, brush height, and average helical content.

Free Energy of Mixing for Helices and Coils. In order to calculate the local free energy of mixing in the helix−coil brush, a lattice model for an athermal mixture of rigid rods and random coils will be used.[21−23] This model may seem contradictory to the assumption in the previous section of helices as wormlike chains but may be reconciled by the idea that a section of wormlike chain much shorter than its persistence length can be approximated as a rigid rod. While this assumption neglects correlations along the length of the helix for the purposes of balancing osmotic repulsion with stretching, this is a well-known shortcoming of lattice models in general and the coil segments of the chain suffer from the same problem.[29,30] For a random-coil brush, neglecting intrachain correlations leads to an accurate prediction of brush height but not the energy required to compress the brush. Here, this assumption is made in order to qualitatively describe the relevant physics of the helicogenic brush with the knowledge that an accurate quantitative model would have to account for intrachain correlations in conjunction with cooperative helix formation as was previously discussed. Nevertheless, the assumptions made here lead to interesting predictions regarding the helical content and density profiles in the brush and are a valid approach to the ultimate goal of a predictive model.

In order to proceed, a region of brush may be described as a mixture of solvent and polydisperse chains that each contain one helical, rodlike domain of length $m\theta$ and one coil domain of length $m(1-\theta)$ where m is an arbitrary length of chain as shown in Figure 1A. Note that m is used here for the length of a chain segment to avoid confusion with the position along a chain, n. Each rod has an orientation specified by an angle, ψ, with the domain axis (i.e., the surface normal). This rod may be placed onto a lattice by breaking it into $y = m\theta \sin\psi$ smaller submolecules that align parallel with the domain axis as depicted in Figure 1B. In the treatment of this system by Flory and Abe, rods may assume a range of angles and the equilibrium value of ψ is that which maximizes the partition function.[21,22] The situation here is somewhat different because the assumption of highly stretched chains, with a trajectory determined by their starting height, fixes $\psi = \cos^{-1}(dz/m\theta)$. Using Buhot and Halperin's variational approximation to the wormlike chain model, the distance traveled in the stretching direction (dz) by a helical segment of chain ($m\theta$) is, on average, given by $dz/(m\theta) = L(\alpha)$.[13] This leads to the expression given for $\hat{y} = y/(m\theta)$ in eq 13. Here, α can be expressed as a function of $\dot{z}$ using eqs 9 and 10 and $\dot{z}$ is a function of z for a given chain starting at a height of ζ ($z \le \zeta \le h$). In eq 9, θ is assigned its equilibrium value, θ^*, which is also a function of z for a chain starting at ζ with the use of 8 through 12.

$$\hat{y} = \sqrt{1 - L^2(\alpha)} \tag{13}$$

With the orientation of the helical segment of a chain specified, it is possible to calculate the interaction energy for a mixture of helical and coil segments. To do this, imagine a volume element of brush that is composed of a distribution of chains of equal length (m) that can assume any of i states specified by their fraction of helical monomers, θ_i, and order parameter, y_i. Each chain consists of one helical segment and one coil segment. The volume of the coil segment relative to the volume of a hypothetical solvent molecule is given by $r_{c,i}$ while that of the helical segment is $r_{h,i}$. The volume of a hypothetical solvent molecule is chosen to match that of one monomer. For this work, the monomer volume is assumed to be the same in the helical and coil states. While helix formation shrinks the effective contour length of a chain, it also "widens" the chain and the overall monomer volume changes only slightly. Because monomer asymmetry and a slight monomer volume decrease in the helical state are believed to be secondary effects that will not change the broad trends seen in brush micro- or macrostructure, they will be ignored for simplicity. However, modeling real experimental data with quantitative accuracy may ultimately require these effects to be incorporated.

The total system volume, v_o, is given by $v_o = v_s + \sum v_i(r_{h,i} + r_{c,i}) = v_s + m\sum v_i$ where m is the chain length in "solvent units" and v_s and v_i are the number of solvent molecules and chains in state i, respectively. The partition function for a polydisperse mixture of rods and coils[21,22] may be given in eq 14:

$$z = \frac{v_o - \sum v_i(r_{h,i} - y_i))!}{v_s!\Pi(v_i!)^2 v_o^{\sum v_i(r_{c,i} + y_i - 2)}} \tag{14}$$

Here, the partition function considers only combinatory factors and neglects the internal configurations (i.e., single chain entropy, outside of the brush) of the helix or random-coil portions. These internal configurations have already been accounted for in the elastic energy through the wormlike chain and freely jointed chain models. Use of Stirling's approximation for large factorials leads to an expression for the free energy of an athermal mixture:

$$\begin{aligned} F_{\text{int}} &= -\ln Z \\ &= v_s \ln v_s - v_s + 2\sum v_i \ln v_i - 2\sum v_i + \sum v_i(r_{c,i} + y_i - 2)\ln v_o \\ &\quad - (v_o - \sum v_i(r_{h,i} - y_i))\ln(v_o - \sum v_i(r_{h,i} - y_i)) + v_o - \sum v_i(r_{h,i} - y_i) \end{aligned} \tag{15}$$

Dividing eq 15 by v_o and making the substitutions, $\theta_i = r_{h,i}/m$, $\phi_i = m v_i/v_o$, $\hat{y}_i = y_i/(\theta_i m)$, and $v_s/v_o = 1 - \Sigma\phi_i$ yields eq 16 for the free energy per site:

$$\begin{aligned} F_{\text{int}}|_{site} &= (1 - \sum\phi_i)\ln(1 - \sum\phi_i) + \frac{2}{m}\sum\phi_i \ln\frac{\phi_i}{m} \\ &\quad + \sum\phi_i\left[1 - \frac{2}{m} - \theta_i(1 - \hat{y}_i)\right] \\ &\quad - [1 - \sum\phi_i\theta_i(1 - \hat{y}_i)]\ln[1 - \sum\phi_i\theta_i(1 - \hat{y}_i)] \end{aligned} \tag{16}$$

The fraction of chains of species i is given by p_i such that $\phi_i = \phi p_i$ where ϕ is the total monomer volume fraction at a given position

and $\Sigma p_i = 1$. The per-site free energy is then given by eq 17 with the function, λ, defined in eq 18:

$$F_{\text{int}}|_{site} = (1-\phi)\ln(1-\phi) + \phi(1-\lambda) - (1-\lambda\phi)\ln(1-\lambda\phi) - \frac{2\phi}{m}\left(1 - \ln\frac{\phi}{m} - \sum p_i \ln p_i\right) \quad (17)$$

$$\lambda = \sum p_i \theta_i (1-\hat{y}_i) \quad (18)$$

Taking the long-chain limit ($m \gg 1$) allows the last term in eq 17 to be neglected. Although it may seem contradictory to take the long chain limit for an arbitrary segment of chain, neglect of the logarithmic terms has the effect of ignoring the placement of chain ends. This is reasonable given that each chain segment is connected to the larger chain and individual segment ends cannot be independently placed. Neglect of the $2\ \phi/m$ term eliminates a trivial constant when eq 17 is substituted into eq 3.

Taking the functional derivative with respect to ϕ of eq 17 in the long-chain limit yields:

$$V(\phi) = -\frac{\delta(F_{\text{int}}|_{site})}{\delta\phi} = \ln(1-\phi) - \lambda\ln(1-\lambda\phi) \quad (19)$$

Regarding the function, λ, it represents the fraction of monomers that have been confined to helices and oriented with the domain axis. Once oriented, these monomers no longer contribute independently to the number of states available to the system. An increase in λ decreases $V(\phi)$, allowing higher densities to be obtained in a brush with a greater fraction of oriented helical monomers. In the limit of completely helical chains that are perfectly oriented, $\lambda = 1$ and $V = 0$. In the opposite limits of completely random-coil or unoriented chains, $\lambda = 0$ and $V = \ln(1-\phi)$ as expected for a random-coil chain. It should be noted that eq 4 is only valid if the osmotic pressure is zero at $\phi = 0$.[15] Using the long chain limit of eq 17, this is indeed found to be the case where the osmotic pressure is calculated as $\phi^2[\delta(F_{int}/\ \phi)/\mathrm{d}\phi]$.

In order to calculate λ, θ_i and $\hat{y}_i$ must be defined at z for a given chain starting at height ζ. Consequently the states, i, are defined by ζ and subscripts on θ and $\hat{y}$ will be changed to reflect this. Here, it is important to point out that while eqs 12 and 13 apply to only a single chain, all chains starting at a given height (ζ) have the same values of θ and $\hat{y}$ at a given position (z) in the brush. The brush is then constructed by bringing together chains that start at different heights, with the number of chains starting at a given height given by eq 7.

Remembering that $\Delta U = U(\zeta) - U(z)$, eq 1 and eqs 8−12 may be solved to express θ_ζ in terms of ΔU which may be subsequently converted to real space after $U(z)$ is determined from integration of $f(U)$. Similarly, $\hat{y}_\zeta$ may be found from eqs 1 and 13 in combination with 8-10. With these parameters defined for each chain, λ may be calculated by summing the contributions from each chain that passes through z. With a continuous distribution of states that are defined by the starting height of each chain, the summation in eq 17 may be converted to an integral as shown in eq 19 where both p_ζ, θ_ζ, and $\hat{y}_\zeta$ are functions of z, h, and ζ:

$$\lambda(z,h) = \int_z^h p_\zeta \theta_\zeta (1-\hat{y}_\zeta)\ \mathrm{d}\zeta \quad (20)$$

With the probability distribution of chain ends specified in eq 7, p_ζ can be calculated using eq 21.

$$p_\zeta = \varepsilon(\zeta,h) \Big/ \int_z^h \varepsilon(\zeta,h)\ \mathrm{d}\zeta \quad (21)$$

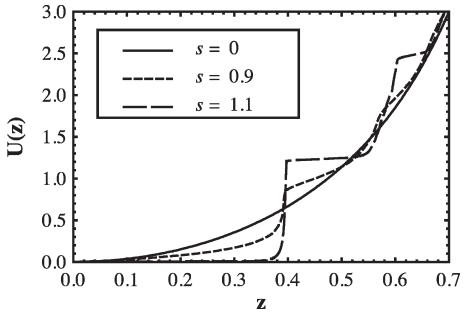

Figure 2. The effective potential, $U(z)$ is shown as a function of z for different values of the Zimm−Bragg parameter, s. When compared to a pure random-coil ($s = 0$), helicogenic brushes show jumps and plateaus in the effective potential that are consequences of the helix−coil transition.

Additionally, the average fraction of helical monomers, $\langle\theta\rangle$, and average orientation parameter, $\langle\hat{y}\rangle$, are defined in eqs 22 and 23.

$$\langle\theta\rangle = \int_z^h p_\zeta \theta_\zeta\ \mathrm{d}\zeta \quad (22)$$

$$\langle\hat{y}\rangle = \int_z^h p_\zeta \hat{y}_\zeta\ \mathrm{d}\zeta \quad (23)$$

Calculation of Brush Properties. With both $V(z)$ and $V(\phi)$ specified, it is possible to solve eq 4 for $\phi(z)$ and other brush properties. This must be done numerically because $V(z)$ is not an analytical function and calculation of $V(\phi)$ requires the calculation of a density profile in order to specify λ. In order to proceed, a trial profile is first assumed for $\lambda(z)$. The brush height, density profile, and distribution of chain ends are subsequently determined, allowing a new calculation of λ. This procedure is repeated until the density profile converges. While it is possible to use any one of the brush parameters (i.e., ϕ, λ, or ε) to check for convergence, only one is necessary as they are interdependent. The difference between the old and new profiles, Δ, is used to assess convergence. The function, $\Delta = |\phi_{new} - \phi_{old}|/\phi_{old}$, is evaluated over z and both the maximum value and the integral of this function are calculated. Because of the uncertainty introduced in the calculation of f in eq 2, the converged solution oscillates about its converged value by 1−2% and both maximum and integrated values of Δ reach steady, nonzero values that reflect this. The converged solution is therefore taken as the average of the two oscillating solutions. This precision is more than sufficient for qualitative analysis and most likely introduces no greater quantitative error than either the use of a lattice model for the interaction energy or the assumption of strong stretching at the brush edge.

RESULTS AND DISCUSSION

Effective Potential as a Function of Zimm−Bragg Parameter. The effective potential, $U(z)$ was evaluated for three different values of the Zimm−Bragg parameter, s = 0, 0.9, 1.1, and these results are shown in Figure 2. For $s = 0$, $U(z)$ rises smoothly from 0. In contrast, plateaus are observed for $s = 1.1$ and $U(z)$ zigzags above and below the $s = 0$ curve with the magnitude of these differences decreasing with increasing z. While plateaus are again apparent for $s = 0.9$, they are much less prominent than for $s = 1.1$. These plateaus are the result of the helix−coil

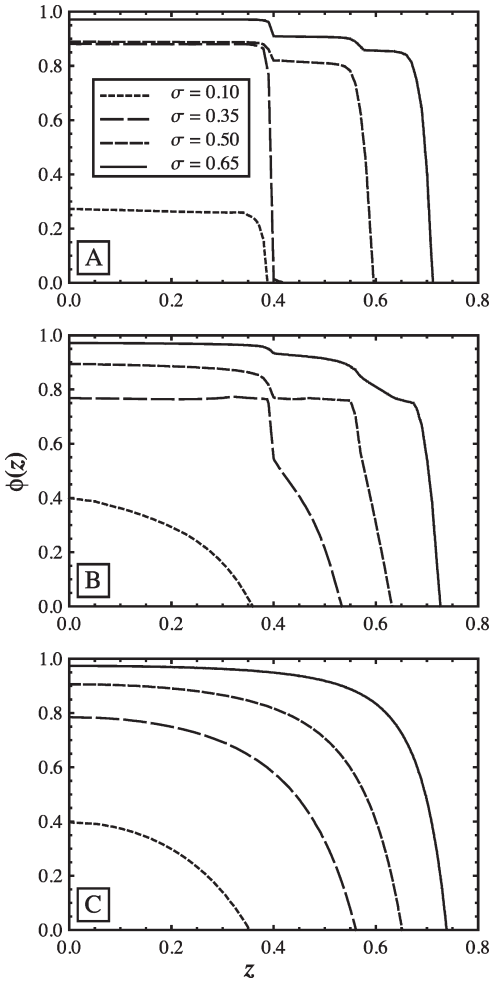

Figure 3. Monomer density is shown as a function of position in the brush for different grafting densities in each plot. Each plot represents a different value of the Zimm−Bragg parameter: (A) $s = 1.1$, (B) $s = 0.9$, (C) $s = 0$. Distinct density layers appear for $s > 0$ while smooth density profiles are observed for the pure random-coil case ($s = 0$).

transition and while the physical significance of multiple plateaus will be demonstrated to have a profound effect on the brush properties, for now they can be understood as a mathematical consequence of having discontinuities in the first derivative of $\dot{z}(\Delta U)$ as was previously discussed.

Brush Microstructure. The helicogenic brush was evaluated for the three values of the Zimm−Bragg parameter discussed above. The case of $s = 0$ corresponds to a chain incapable of helix formation while $s = 0.9$ and 1.1 correspond to weak aversion and propensity for helix formation, respectively. Monomer density profiles for each case are shown in Figure 3 at several grafting densities. The most striking feature of the brushes capable of helix formation is the appearance "layers" of different densities. At low grafting density, only one layer is present but as grafting density increases, a second, and eventually a third, layer appears. Polymer density remains roughly constant within a layer but decreases from the inner to outer layers. Helix formation must be responsible for these unique features as layer formation is not observed for $s = 0$.

The average helical content profile, $\langle\theta\rangle$, is shown in Figure 4 for $s = 0.9$ and 1.1. Again, distinct layers in average helical content are seen that correspond to the changes in density profile. Whereas density decreases when moving toward the exterior

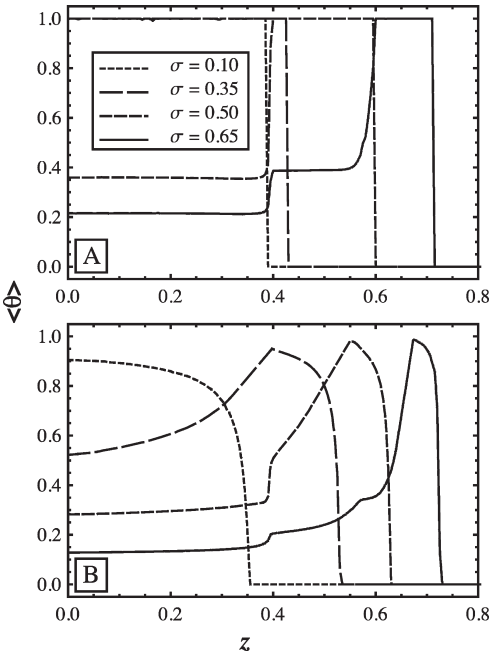

Figure 4. The average helical fraction is shown as a function of position in the brush for different grafting densities in each plot. Each plot represents a different value of the Zimm−Bragg parameter: (A) $s = 1.1$; (B) $s = 0.9$.

layers of the brush, helical content increases when moving to progressively exterior layers (when multiple layers exist, for $\sigma = 0.35$, 0.50, and 0.65). This can be explained by the ability of a helix to unravel in response to high stretching as described by Buhot and Halperin.[13] As grafting density increases and crowding-induced stretching becomes high, some chains partially convert to random-coils in an inner layer and extend to an outer layer to alleviate crowding. In the outer layer, however, crowding and stretching is less and helices are again favored. Note that at all densities, for $s = 0.9$, helical content decreases near the top of the outermost layer as the chain returns to its natural random-coil state in the absence of stretching.

It should be noted that the use of low, moderate, and high stretching in this discussion is separate from the use of "strongly stretched" to describe chains for which fluctuations about their most probable trajectory may be neglected. Except where otherwise noted, low, moderate, and high stretching are used to describe the relationship between stretching and either the helix−coil transition or the alignment of helices. As has already been discussed, it is assumed that crowding-induced stretching is sufficiently strong to ensure model validity everywhere except the very outer regions of the brush.

In order to better understand these "helical layers", it is helpful to look at the helical content profiles of individual chains starting at different heights. This is shown in Figure 5 for nonzero s values. For a chain starting inside the first (innermost) layer at $\zeta = 0.38$, it is completely helical for $s = 1.1$ where the helical state is preferred at low to moderate degrees of stretching. For $s = 0.9$, a high degree of helical content is also observed. While low stretching is insufficient to induce helix formation, the moderate stretching experienced by the chain just below its starting point is sufficient to favor helices.

A stretching-induced increase in random-coil content is observed in chains that originate in the second layer ($\zeta = 0.55$).

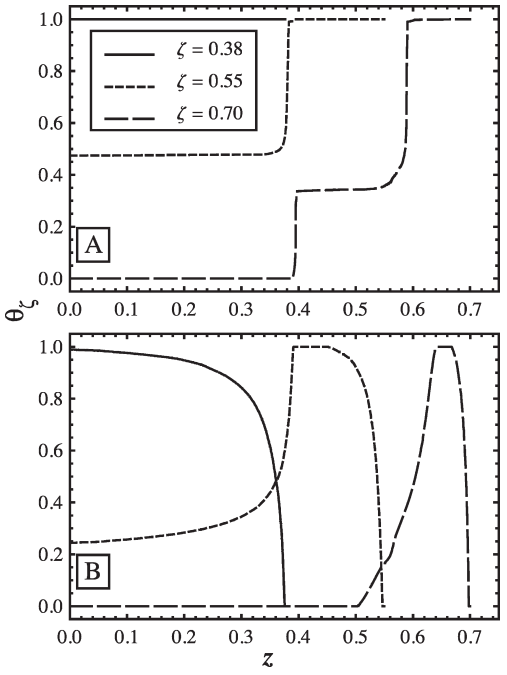

Figure 5. Helical fraction is shown as a function of position in the brush for individual chains starting at different heights, ζ. (A) For $s = 1.1$, chains are completely helical in their starting height and partially convert to random-coils each time they move through one of the inner layers. (B) For $s = 0.9$, chains are random-coils near their starting height but quickly form helices that are stabilized by moderate stretching within their starting layer.

For $s = 1.1$, the chain is completely helical in the second layer but helices partially unravel as the chain passes through the first layer. This preference for the random-coil state is a consequence of finite extensibility of the helix, which may only reach a height of 0.4 when completely helical and oriented. The picture is more complicated for $s = 0.9$ where the chain is a random-coil at its starting height, forms a helix as it descends through the second layer, remains highly helical near the top of the first layer, and returns to the random-coil state gradually as it moves toward the surface. The chain starts out in the random-coil state because stretching is weak near its starting height and random-coils are preferred in the absence of stretching for $s < 1$. Some moderate amount of stretching helps the chain form helices as it descends to and through the higher portions of the first layer. At some point in the first layer, stretching becomes too great and the chain again prefers the random-coil state for the same reasons discussed in the case of $s = 1.1$. Similar trends are observed for a chain starting at $\zeta = 0.70$ with the main change being the inverse relationship of θ in the lower layers with increasing starting height. Again, finite extensibility requires that a chain starting higher in the brush must exist more in the random-coil state to reach the surface from that height. A cartoon of these phenomena is shown in Figure 6 in order to highlight the main points of the above discussion.

As was demonstrated by Shim and Cates for a random-coil, finite extensibility results in a more sharply peaked distribution of chain ends than if a Gaussian elasticity model is assumed.[15] This effect is magnified for the helicogenic brush where finite extensibility of both helices and chains is coupled with the ability to easily orient helices perpendicular to the grafting surface. Figure 7 shows the distribution of chain ends for all cases studied. For $s = 0$,

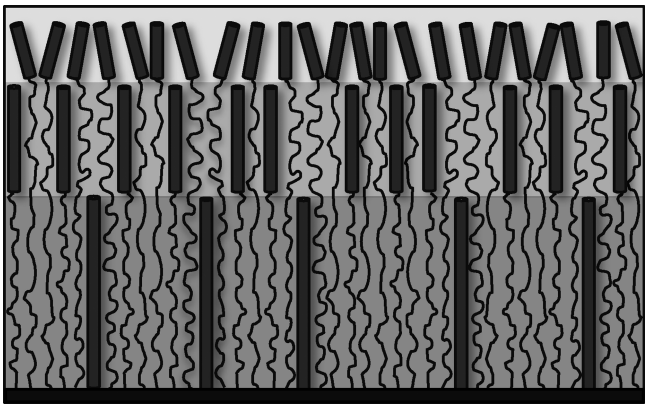

Figure 6. Simplified picture of the multilayer brush structure depicted for high tethering density for $s = 1.1$, where helices are depicted as rods. The outermost layer is least dense but remains completely helical. Helices are well-oriented throughout the brush but are most disoriented in the outermost layer. Chains must enter the random-coil state to extend into the outer layers causing the average helical content to decrease when moving from outer to inner layers. More subtle features of the brush are not shown such as partial helix formation along a chain within a layer and the placement of chain ends at locations other than layer boundaries.

the distributions are qualitatively similar to those found by Shim and Cates but differ quantitatively due to the differences between the ad hoc elasticity model used in their work and the freely jointed chain model used here. For $s > 0$, sharp peaks in the end distribution are observed near the edges of brush layers observed in Figure 3. While there are sharp peaks in the distribution, it is important to note that the end distribution is nonzero everywhere throughout the brush and thus the given distribution is globally stable.[14] At first glance, this end distribution suggests that the helicogenic brush may be treated with the less complicated Alexander model that assumes uniform chain stretching and step-like density profiles. However, these results also demonstrate that a proper treatment of a helicogenic brush must account for multiple layers of brush and appropriate correlations between layers. It is not obvious that this is possible by simply stacking "uniform" brush layers on top of one another, as the Alexander model would require. This observation helps to justify the added difficulty of using the present model for a helicogenic brush.

To close out the discussion of microscopic brush properties, it should be noted that helices, once formed, are almost all well-oriented normal to the grafting surface. This is due to the ease with which helices are oriented in the stretching direction. The orientation angle is calculated from $\psi = \sin^{-1} \hat{y}$ and for weakly stretched chains near their starting height, $\hat{y} = 1$ and $\psi = 90°$. As the chain extends toward the surface, $\hat{y}$ decays rapidly such that $\psi < 15°$ almost immediately below the starting point for most chains. Thus, if a helix does form, it is well-oriented except in the region very near its starting height. While this sharp transition in orientation is physically prohibited by the large persistence length of a wormlike helix, this region of disorientation is so small that it is has a negligible effect on the overall model.

Macroscopic Brush Properties. As was apparent in the preceding section, there is a strong interconnection between helix formation and brush properties. Chain stretching induced by brush crowding served to either favor helices or random-coils at different points along an individual chain. In turn, helix formation resulted in well-defined layers of relatively uniform

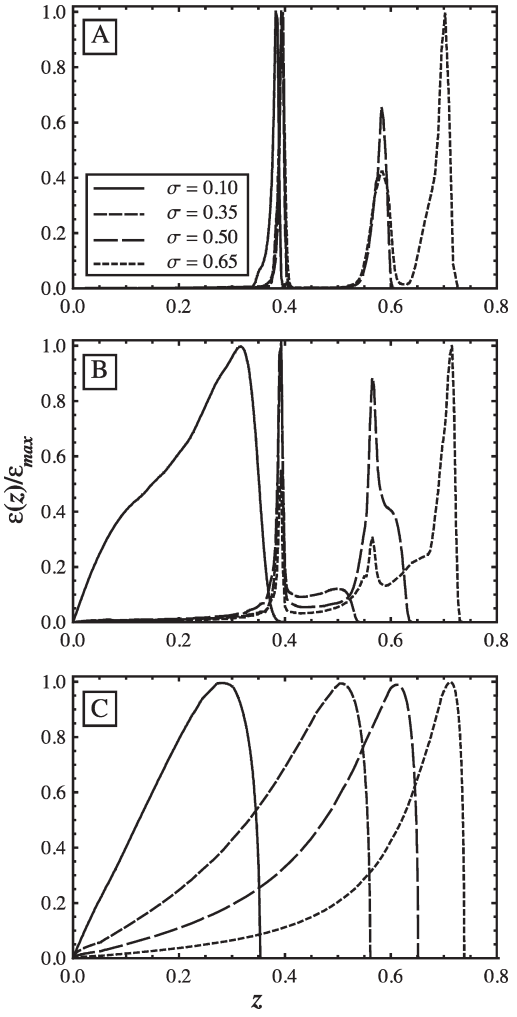

Figure 7. Distribution of chain ends shown as a function of position in the brush for (A) $s = 1.1$, (B) $s = 0.9$, and (C) $s = 0$. Each distribution has been normalized by its maximum value.

density and helical content. This section will explore the macroscopic effect of brush formation on the helix−coil transition as well as the effect of helix formation on brush height and lateral compressibility.

Crowding-induced stretching was demonstrated to both stabilize helix formation at low-to-moderate degrees of stretching, and then to unravel more highly stretched helices. The amount of stretching experienced by an individual chain varied with its starting height and along the length of the chain. Furthermore, there is a continuous distribution of chain ends as shown in Figure 7. These effects may be combined to get an average fraction of helical monomers for the entire brush by counting the total number of monomers in the helical state relative to the total number of monomers. This global average, Θ, is given by eq 24 and is shown as a function of grafting density in Figure 8.

$$\Theta = \frac{1}{\sigma}\int_0^h \mathrm{d}z\,\langle\theta\rangle\phi(z) \qquad (24)$$

For $s = 1.1$, $\Theta = 1$ for $\sigma < 0.4$ on account of the fact that increasing tethering density serves mainly to better orient already formed helices in a single layer. Further increases in grafting density cause a second layer to form, with concomitant helix

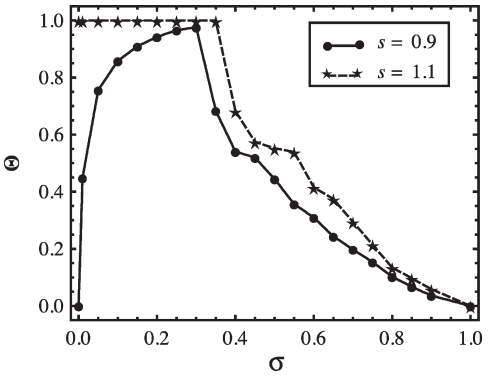

Figure 8. Globally averaged helical fraction shown as a function of tethering density for $s = 0.9$ and 1.1.

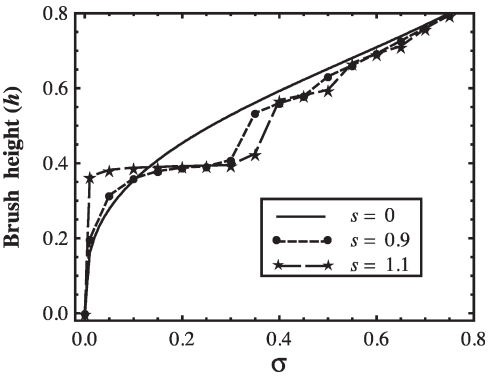

Figure 9. Brush height is shown as a function of tethering density for $s = 0$, 0.9, and 1.1.

formation and extension of some chains from the first layer into the second. As the grafting density approaches unity, chains are stretched to their full contour length and a complete return to the random-coil state is observed. The undulations in the decay of Θ are due to the formation of successive layers as was previously discussed. The situation for $s = 0.9$ is similar to $s = 1.1$ for high grafting densities. However, a return to the random-coil state begins at slightly lower σ because it is easier to unravel helices at lower s. The main difference for $s = 0.9$ is seen at low σ and is due to the fact that the natural state of a single chain is to remain in the random-coil state. As σ increases from 0, Θ rises sharply at first and levels off just below complete helix formation near $\sigma = 0.3$ before decreasing again as discussed above.

Helix formation has a profound effect on the brush as well. Brush height is shown as a function of tethering density in Figure 9 for $s = 0$, 0.9, 1.1. In comparison to the random-coil brush height, that of the helicogenic brushes rises faster at low tethering densities, with the more helicogenic brush ($s = 1.1$) rising much faster than for $s = 0.9$. While helices tend to orient normal to the grafting surface at even low σ, the fact that helix formation is complete for $s = 1.1$ while stretching is required to induce helix formation for $s = 0.9$ causes the height of the latter case to more closely resemble a random-coil. Following the initial rise, brush height remains relatively constant as σ increases on account of the fact that helical content in both types of brush is high and helices are becoming more oriented but not extending past the contour length of the helix. In this region, the random-coil brush height surpasses the helicogenic brush due to the longer contour length of the coil versus the helical state. A further

dx.doi.org/10.1021/ma200782e |*Macromolecules* 2011, 44, 4977–4987

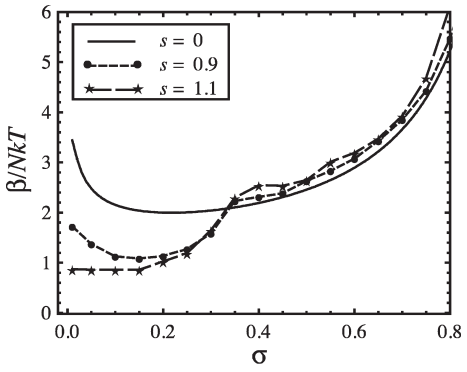

Figure 10. Lateral compressibility shown as a function of tethering density for s = 0, 0.9 and 1.1.

increase in tethering density requires helices to partially unravel and form multiple layers, allowing the helicogenic brush height to approach that of the random-coil brush in a series of successively smaller jumps and successively more sloped "plateaus". By σ = 0.6, helices are nearly completely unraveled and is brush height is almost indistinguishable from the random-coil case.

The Zimm−Bragg parameter, s, is a function of temperature given that Δg includes both entropic and enthalpic contributions. Assuming that enthalpic contributions favor the helical state, s should decrease with temperature, down to a minimum value determined by the entropic contributions. Thus, brush height should be a function of temperature for regions in Figure 9 where brush height depends on s. In particular, brush height should decrease with increasing temperature for $\sigma < 0.1$, increase with temperature for $0.15 < \sigma < 0.6$, and remain relatively temperature-independent for $0.1 < \sigma < 0.15$ and $\sigma > 0.6$. These predictions provide opportunities to experimentally verify this model.

Helix formation also has the effect of lowering the overall free energy of the brush. As this work is partially motivated by the effect of helix formation on geometry in self-assembled systems, the more useful quantity is the lateral compressibility defined by $\beta = dF_{br}/d\sigma$. This force represents the resistance of the brush to an increase in tethering density and can be balanced against forces that favor increased density such as dispersion and hydrophobic forces in the core of hydrophobically driven self-assembled structures. The compressibility is shown as a function of tethering density in Figure 10 where it can be seen that helix formation lowers β for $\sigma < 0.3$. Thus, a helicogenic brush is more amenable to higher σ in this region and this fact leads to a lower effective headgroup area when considering the packing parameter to predict micelle geometry.[8] As the tethering density increases above σ = 0.3 and helices are forced to unravel and extend to form multiple layers, it becomes harder to compress a helicogenic brush relative to a random-coil brush although this effect is not as dramatic as the decrease seen in β for $\sigma < 0.3$. Note that in all cases, $\beta > 0$ and so the brush is unstable with respect to σ (i.e., the minimum in F_{br} is found at $\sigma = 0$) in the absence of compressive forces. Future work will incorporate curvature effects into the model developed here in order to better predict shape transitions in self-assembled systems.

The use of self-consistent field theory to treat helicogenic polymer brushes has a number of advantages over more analytically tractable models. First is the more realistic assumption of nonuniform stretching along the length of the chain. This assumption has led to the prediction of multiple layers in densely grafted brushes in which density and helical content remain relatively constant within a layer but may change sharply between layers. Second, the finite extensibility of both coils and helices is generally regarded as more accurate than the infinite extensibility of Gaussian chains. Finally, the rigorous development of a form for the interaction energy of a brush with partial helical content is believed to be more accurate than ad hoc treatments previously used for this purpose. Taken together, these features of the current model likely present the most accurate picture of a helicogenic brush to date and have made interesting predictions regarding the microscopic and macroscopic brush properties.

One area for improvement of the current model is to address the interrelated issues of short-range correlations along the chain in addition to cooperativity in the helix−coil transition. The former problem is a well-understood shortcoming of the lattice approach for random coils and is handled by scaling concepts, which assume a correlation blob in which ideal chain statistics are unperturbed by the brush. It is difficult to imagine a similar strategy working here because a mixture of rods and coils is not self-similar (i.e., characterized by a single fractal exponent) on all length scales, a requirement for scaling methods. In addition, cooperative helix formation may affect the length scale of correlations along an individual chain. While the effect of cooperative helix formation should be considered alongside any approach to address chain correlations in the elastic or interaction energies, it is also possible that the helix−coil transition is less cooperative in a brush than for peptides and proteins in solution for the reasons discussed in the development of eq 11. In any case, it seems there are several unresolved issues regarding intrachain correlations and cooperative helix formation which merit further experimental and theoretical consideration.

Additionally, this work only considered an athermal mixture of helices and coils, neglecting solvent quality and other enthalpic effects. It is not hard to generalize eq 17 to include pairwise enthalpic interactions for a ternary mixture of helix, coil, and solvent. In this case, the methods used in this work remain unchanged with the exception that a different, analogous version of eq 4 must be used if the pairwise interactions are such that the osmotic pressure is minimized for nonzero values of ϕ. This situation is discussed in further detail in the work of Shim and Cates.[15]

Pairwise enthalpic attractions between helical monomers may also be useful to address a propensity for helices to aggregate, particularly when specific peptide sequences exhibit amphipathic behavior in the helical state.[31,32] Helical aggregation could cause lateral phase separation into regions of high and low helical content that would behave very differently from each other. For now, neglect of helical aggregation seems to be a good general assumption, particularly for the experimental system of Gebhardt et al. where polylysine brushes exhibited structure that was characteristic of α-helices rather than coiled-coils. This distinction can be made by comparing the magnitudes of the minima in their circular dichroism spectra at 208 and 222 nm. Both minima are indicative of helical content but the minimum at 222 nm becomes deeper for coiled-coils.[33]

CONCLUSIONS

This work describes the physics of a helicogenic polymer brush and demonstrates that crowding-induced stretching in the brush affects the helix−coil transition. At low-to-moderate

tethering densities, helix formation is stabilized in chains that would otherwise prefer the coil state. Strong stretching at high tethering densities can force the helix to unravel as the chain is forced to extend in order to relieve crowding. This extension results in distinct layers in the brush in which monomer density and helical content are relatively constant but there are sharp transitions in these properties between layers. Helix formation and orientation makes the brush more amenable to lateral compression at low-to-moderate tethering densities because of fewer repulsive monomer−monomer interactions once monomers are sequestered into well-oriented helices. However, the above-mentioned layer formation resists lateral compression to high tethering densities as layer formation requires helix unraveling. Furthermore, finite extensibility in both helices and random-coil portions of chain causes chain ends to concentrate in the outer regions of each layer.

While brush-induced stabilization of helix formation and increased lateral compressibility of helical brushes are not surprising results given previous experimental observations, this model is believed to be the most quantitative description of the helicogenic brush to date and some of its more subtle features may be useful in understanding and predicting the behavior of self-assembled materials. For example, resistance to lateral compression at high tethering density, and the unraveling of helices that leads to this phenomenon, may explain why wormlike micelles were observed in the work of Tu et al.[9] instead of vesicles or structures with negative curvature. Another subtle feature of the helicogenic brush is the observation that moderate stretching in the outermost layer can stabilize helix formation in this layer even if the rest of the chains are mostly random-coils (cf. Figure 5B, $\zeta = 0.70$). Thus, if helical content is important to biofunctionality, the region of the brush that is exposed to the environment will remain helical even though the overall helical content of the brush is low.

Future work in this area will address the effects of curvature in order to predict shape transitions in self-assembled structures, such as micelles, with helicogenic capabilities. In addition to curvature effects, predictive accuracy of the current model may be limited by neglect of intrachain correlations both from the perspective of the elastic and interaction energies as well as in cooperative helix formation. As these are difficult issues to address theoretically, this work hopes to motivate experimentation on helicogenic brushes that may guide further advances in the current model. Some of the features predicted here, such as relatively sharp density transitions between regions of the brush and temperature dependence of brush height, should be observable in appropriately designed neutron or X-ray reflectivity experiments.

AUTHOR INFORMATION

Corresponding Author

*E-mail: mark.kastantin@colorado.edu.

ACKNOWLEDGMENT

This work was supported by National Heart, Lung and Blood Institute Grant U01 HL080718, National Institute of General Medical Sciences Grant 1F32GM091777-01, and by the MRSEC Program of the National Science Foundation under Award DMR05-20415. The authors also wish to thank Professor Glenn Fredrickson for helpful discussions on self-consistent field theory.

TABLE OF SYMBOLS

symbol	description
a	random-coil monomer length
a_h	helical monomer length
A	energy of a chain starting very near the grafting surface
b	stretching force
f	dz/dU
F	nondimensional free energy
Δg	per-monomer free energy for the helix−coil transition
h	nondimensional brush height
k	Boltzmann constant
L	Langevin function
L_{int}	integrated Langevin function
m	nondimensional polymer segment length
n	nondimensional position along a chain
N	number of monomers in a polymer chain
p_i	probability of observing a chain in state i
r	number of lattice sites for one species
s	Zimm−Bragg parameter
t	dimensional position along a chain
T	absolute temperature
U	same as V (below) to within an arbitrary function of brush height
v	number of species
v_o	total number of lattice sites
V	space-dependent monomer potential
x	nondimensional stretching force
y	orientational parameter for helices
$\hat{y}$	nondimensional orientational parameter
$\langle\hat{y}\rangle$	locally averaged nondimensional orientational parameter
z	nondimensional coordinate normal to the grafting surface
$\dot{z}$	dz/dn
Z	coordinate normal to the grafting surface
α	force-dependent variational parameter for a wormlike helix
β	lateral compressibility
γ	a/a_h
Δ	difference function used to check convergence
ε	distribution of chain ends
ζ	nondimensional starting height of an individual chain
η	persistence length of helices in monomer units
θ	helical fraction
$\langle\theta\rangle$	locally averaged helical fraction
Θ	globally averaged helical fraction
λ	fraction of "oriented" helical monomers
ρ	monomer number density
σ	nondimensional tethering density
Σ	dimensional tethering density
ϕ	monomer volume fraction
ψ	angle of the helical axis with the domain axis

REFERENCES

(1) Versluis, F.; Marsden, H. R.; Kros, A. *Chem. Soc. Rev.* **2010**, *39*, 3434–3444.

(2) Zhao, X. B.; Pan, F.; Xu, H.; Yaseen, M.; Shan, H. H.; Hauser, C. A. E.; Zhang, S. G.; Lu, J. R. *Chem. Soc. Rev.* **2010**, *39*, 3480–3498.

(3) Olsen, B. D.; Segalman, R. A. *Mater. Sci. Eng. R-Rep.* **2008**, *62*, 37–66.

(4) Gebhardt, K. E.; Ahn, S.; Venkatachalam, G.; Savin, D. A. *Langmuir* **2007**, *23*, 2851–2856.

(5) Gebhardt, K. E.; Ahn, S.; Venkatachalam, G.; Savin, D. A. *J. Colloid Interface Sci.* **2008**, *317*, 70–76.
(6) Lin, J. P.; Zhu, G. Q.; Zhu, X. M.; Lin, S. L.; Nose, T.; Ding, W. W. *Polymer* **2008**, *49*, 1132–1136.
(7) Yang, C. T.; Wang, Y. L.; Yu, S.; Chang, Y. C. I. *Biomacromolecules* **2009**, *10*, 58–65.
(8) Israelachvili, J. N., *Intermolecular and surface forces.*, 2nd ed.; Academic Press: Amsterdam and Boston, MA, 1992; p xxi, 450 p.
(9) Tu, R. S.; Marullo, R.; Pynn, R.; Bitton, R.; Bianco-Peled, H.; Tirrell, M. V. *Soft Matter* **2010**, *6*, 1035–1044.
(10) Shimada, T.; Lee, S.; Bates, F. S.; Hotta, A.; Tirrell, M. *J. Phys. Chem. B* **2009**, *113*, 13711–13714.
(11) Yu, Y. C.; Berndt, P.; Tirrell, M.; Fields, G. B. *J. Am. Chem. Soc.* **1996**, *118*, 12515–12520.
(12) Buhot, A.; Halperin, A. *Europhys. Lett.* **2000**, *50*, 756–761.
(13) Buhot, A.; Halperin, A. *Macromolecules* **2002**, *35*, 3238–3252.
(14) Milner, S. T.; Witten, T. A.; Cates, M. E. *Macromolecules* **1988**, *21*, 2610–2619.
(15) Shim, D. F. K.; Cates, M. E. *J. Phys. (Paris)* **1989**, *50*, 3535–3551.
(16) Watanabe, H.; Tirrell, M. *Macromolecules* **1993**, *26*, 6455–6466.
(17) Baumgartner, A. Simulations of macromolecules. In *Monte Carlo Method in Condensed Matter Physics, Second, Corrected and Updated Edition*, Springer: New York, **1995**; Vol. *71*, pp 285−316.
(18) Chakrabarti, A.; Toral, R. *Macromolecules* **1990**, *23*, 2016–2021.
(19) Lai, P. Y.; Binder, K. *J. Chem. Phys.* **1991**, *95*, 9288–9299.
(20) Murat, M.; Grest, G. S. *Macromolecules* **1989**, *22*, 4054–4059.
(21) Flory, P. J. *Macromolecules* **1978**, *11*, 1138–1141.
(22) Flory, P. J.; Abe, A. *Macromolecules* **1978**, *11*, 1119–1122.
(23) Flory, P. J.; Ronca, G. *Mol. Cryst. Liq. Cryst.* **1979**, *54*, 289–309.
(24) Zhulina, E. B.; Borisov, O. V.; Priamitsyn, V. A. *J. Colloid Interface Sci.* **1990**, *137*, 495–511.
(25) Skvortsov, A. M.; Gorbunov, A. A.; Pavlushkov, V. A.; Zhulina, E. B.; Borisov, O. V.; Priamitsyn, V. A. *Polym. Sci. USSR* **1988**, *30*, 1706–1715.
(26) Crump, K. S. *J. ACM* **1976**, *23*, 89–96.
(27) Mallet, A. *Numerical Inversion of Laplace Transform*, 0210−968; Wolfram Library Archive: Champaign, IL, 2000.
(28) Freed, K. F.; Dudowicz, J.; Stukalin, E. B.; Douglas, J. F. *J. Chem. Phys.* **2010**, 133.
(29) de Gennes, P.-G., *Scaling concepts in polymer physics*. Cornell University Press: Ithaca, NY, 1979; p 324 p.
(30) Halperin, A.; Tirrell, M.; Lodge, T. P. *Adv. Polym. Sci.* **1992**, *100*, 31–71.
(31) Hartings, M. R.; Gray, H. B.; Winkler, J. R. *J. Phys. Chem. B* **2008**, *112*, 3202–3207.
(32) MacKenzie, K. R.; Prestegard, J. H.; Engelman, D. M. *Science* **1997**, *276*, 131–133.
(33) Greenfield, N. J.; Hitchcockdegregori, S. E. *Protein Sci.* **1993**, *2*, 1263–1273.